The Role of a Longshore Pressure Gradient in Pacific Northwest Coastal Dynamics[1]

FRANCISCO E. WERNER AND BARBARA M. HICKEY

School of Oceanography, University of Washington, Seattle, 98195

(Manuscript received 6 July 1982, in final form 10 November 1982)

ABSTRACT

In this paper we demonstrate the importance of the seasonal barotropic longshore pressure gradient force to Pacific Northwest coastal dynamics. Values of the seasonal longshore pressure gradient corrected for gauge height relative to a level surface (Hickey and Pola, 1982) and for year-to-year variations (Enfield and Allen, 1980) were included in the two-dimensional, time-dependent, baroclinic finite-difference model of Hamilton and Rattray (1978) as an external force. Observed wind stress, stratification and bottom topography were included in the model, and comparisons were made with current meter data in each of the three seasonal situations observed in the Northwest: pressure gradient force southward opposing local wind stress (winter), pressure gradient force northward opposing local wind stress (summer), and pressure gradient force and local wind stress both southward (spring). Three important features of the seasonal circulation are shown to depend on the existence of the pressure gradient force: the northward undercurrent (the California Undercurrent) that exists along most of the West Coast during summer, a southward undercurrent (which we denote the Washington Undercurrent) that the model predicts and observations shown herein substantiate for the Pacific Northwest slope during winter, and the anomalously strong southward flow that occurs subsequent to the spring transition. Finally, the seasonal variation of the balance between wind stress, bottom stress and vertically integrated longshore pressure gradient force as a function of bottom depth is addressed. In particular, it is shown that bottom stress is significant in the mid-shelf region during both winter and spring. The commonly made assumption that offshore transport in the surface layer is balanced by onshore transport in the inviscid interior is shown to be invalid except during summer.

1. Introduction

A longshore pressure gradient has been shown to be essential to the dynamics of coastal circulation along the east coast of the United States (Stommel and Leetmaa, 1972; Scott and Csanady, 1976; Csanady, 1978). Recent papers on West Coast circulation have considered the effect of longshore pressure gradients on cross-shore circulation (Bryden, 1978, for summer 1973), on mean circulation (Hickey, 1981, for late winter 1975), and on the existence of the northward undercurrent that occurs over the shelf and slope during summer (Garvine, 1971; Hurlburt and Thompson, 1973; McCreary, 1981; Philander and Yoon, 1982; Suginohara, 1982; Yoon and Philander, 1982). Hickey and Pola (1982) have described the seasonal oscillation of the observed coastal pressure gradient and its forcing mechanisms from 50 to 20°N along the west coast of the North American continent. They show that the pressure gradient in the Pacific Northwest is primarily determined by nonlocal wind forcing, via the "topographic wave" mechanism of Csanady (1978). The present paper investigates the role of the seasonal barotropic longshore pressure gradient in the coastal dynamics of the Pacific Northwest. In particular, three important features of the mean circulation are discussed: the anomalously strong southward flow that follows the spring transition (Sobey, 1977), the well-documented northward undercurrent (the California Undercurrent) that exists along most of the West Coast in summer (Hickey, 1979), and a southward undercurrent (which we denote the Washington Undercurrent) which the model predicts and observations substantiate for the Pacific Northwest slope during winter.

The dynamics are investigated using the two-dimensional, baroclinic, time-dependent numerical model of Hamilton and Rattray (1978) with the addition of the observed longshore pressure gradient as an exterior forcing term. Although the wind-driven, steady models of Yoshida (1967), Csanady (1978) and McCreary (1981) and the wind-driven, time-dependent models of Philander and Yoon (1982) and Suginohara (1982) describe mechanisms for the set up of longshore pressure gradients along coastlines, none of them consider all the effects (friction, topography, coastal wind forcing, deep ocean currents, heating and cooling) that Hickey and Pola (1982) have shown to be significant to the generation of the seasonal longshore pressure gradient. These effects can be included by treating the pressure gradient as an exterior force. Welander (1957) shows that if the sea surface is regarded as an externally prescribed forcing function,

[1] Contribution No. 1307 from the School of Oceanography, University of Washington, Seattle 98195.

the local velocity profile can be uniquely determined by the local time histories of wind stress and sea surface slope.

The other existing models differ from the present one in several other respects. Csanady (1978) considers only depth-averaged velocities and, thus, is unable to resolve the vertical structure of the currents. The absence of topography in McCreary (1981) and Philander and Yoon (1982) implies that their models are strictly valid only in regions where the internal Rossby radius of deformation is much greater than the shelf width. This condition is never met in the Pacific Northwest, where the shelf width is on the order of 50 km and the internal Rossby radius is on the order of 15 km. The inclusion of topographic effects, as we will show later, will play an important role in understanding the balance of forces on the Washington–Oregon shelf. Suginohara, on the other hand, includes topography and vertical structure but, like McCreary and Philander and Yoon, does not include the effect of bottom friction. Brink (1982) discusses the effect of bottom friction on coastal trapped waves, concluding that if the effect is sufficiently large, the modal decomposition required to find wave solutions is invalid. He points out that, in those cases, a more appropriate approach would be that of Csanady (1978), who determines the mean effect of decaying topographic waves on the circulation and sea level along a coast. The reasonably good agreement between the Csanady model and sea level observations on seasonal scales (Hickey and Pola, 1982) suggests that bottom friction cannot generally be ignored. In view of the limitation of the existing models, the application of observed pressure gradient data as exterior forcing to a model which includes both vertical structure and realistic bottom topography is an approach that can be expected to yield new results.

Since the purpose of this paper is to elucidate seasonal effects, the fluctuating pressure gradient has not been included. The role of the fluctuating pressure gradient in Pacific Northwest coastal dynamics is being investigated in a separate paper. Those diffusive effects that are implicitly neglected when the mean circulation is determined using mean data rather than hourly data, should not significantly affect the comparison of the model results with the averaged observations.

We will first demonstrate how a longshore pressure gradient alters the basic response of a system to local wind driving. We will then describe the relative roles of stratification, topography and spatial variation of the longshore pressure gradient in determining the cross-shore and longshore velocity fields. Last, we will investigate the seasonal variation of the effect of the pressure gradient on Pacific Northwest coastal circulation, using observations to substantiate model predictions.

2. The coastal pressure gradient

The existence of a long term mean longshore pressure gradient along the west coast of the United States was first demonstrated by Reid and Mantyla (1976) using steric height data extrapolated to the coast by the method of Montgomery (1941). Enfield and Allen (1980) presented the seasonal cycle of de-meaned subsurface pressure (tide gauge height plus atmospheric pressure) along the West Coast. Their data were de-meaned because tide gauge data are obtained relative to a gauge height that is an arbitrary height above a level surface. The results are thus *relative to* some unknown long term mean height above a level surface. Recently, Hickey and Pola (1982) added the long term mean steric height (0/500 db) data of Reid and Mantyla (1976) to the de-meaned seasonal subsurface pressure data of Enfield and Allen (1980) to obtain the seasonal variation of "quasi-absolute" subsurface longshore pressure gradient along the West Coast. They show that the principal features of both the seasonal and long term mean pressure gradient force in the Pacific Northwest can be explained by the arrested topographic wave model of Csanady (1978). Thus, sea level height at a particular location is determined not only by the local longshore wind stress but also by the longshore wind stress south of that location. In particular, the lag between the spring onset of southward local wind stress and the onset of northward pressure gradient force occurs because sea level in the Pacific Northwest during spring is primarily determined by the strong southward wind stress off California at that time.

During winter, the pressure gradient force off Washington and Oregon is southward, opposing the northward local wind stress. When the stress decreases during late winter the pressure gradient force decreases, but remains southward through June, one month after the local stress has become southward, so that both wind and pressure gradient forces are in the same direction. A northward pressure gradient force develops in summer, opposing the southward local wind stress. The dynamics and resulting circulation of these three seasonal situations will be explicitly addressed in Sections 5 and 6 of this paper.

3. The model

The model is based on the formulation of Hamilton and Rattray (1978) that was later refined and tested by Hickey and Hamilton (1980). The model equations are

$$\frac{\partial \zeta}{\partial t} + \frac{\partial}{\partial x}\int_{-h}^{\zeta} u\,dz = 0, \tag{3.1}$$

$$w = -\frac{\partial}{\partial x}\int_{-h}^{z} u\,dz, \tag{3.2}$$

$$\frac{\partial u}{\partial t} - fv = -g\frac{\partial \zeta}{\partial x} - \frac{g}{\rho_0}\int_z^{\zeta}\frac{\partial \rho}{\partial x}\,dz + \frac{\partial}{\partial z}\left(A_v\frac{\partial u}{\partial z}\right), \quad (3.3)$$

$$\frac{\partial v}{\partial t} + fu = -g\frac{\partial \zeta}{\partial y} + \frac{\partial}{\partial z}\left(A_v\frac{\partial v}{\partial z}\right), \quad (3.4)$$

$$\frac{\partial \rho}{\partial t} + u\frac{\partial \rho}{\partial x} + w\frac{\partial \rho}{\partial z} - \frac{\partial}{\partial x}\left(K_h\frac{\partial \rho}{\partial x}\right) - \frac{\partial}{\partial z}\left(K_v\frac{\partial \rho}{\partial z}\right) = 0, \quad (3.5)$$

$$\frac{\partial \bar{u}}{\partial t} - f\bar{v} = -g\frac{\partial \zeta}{\partial x} - \frac{g}{H\rho_0}\int_{-h}^{\zeta}\int_z^{\zeta}\frac{\partial \rho}{\partial x}\,dz\,dz + (\tau_{xs} - \tau_{xb})/H, \quad (3.6)$$

$$\frac{\partial \bar{v}}{\partial t} + f\bar{u} = -g\frac{\partial \zeta}{\partial y} + (\tau_{ys} - \tau_{yb})/H. \quad (3.7)$$

The variables are defined in the Appendix.

The model equations (3.1)–(3.7) differ from those used in Hamilton and Rattray (1978) and Hickey and Hamilton (1980) in that a longshore pressure gradient term has been included and the nonlinear terms in the momentum equations have been neglected. Results when the nonlinear terms were included (not shown) were not significantly different from those obtained when they were excluded; in the interest of identifying the governing processes unambiguously, we have chosen to ignore them entirely.

The boundary conditions are such that no normal volume or density fluxes pass through the solid boundaries, $v = 0$ on the vertical solid boundaries and the vertical density flux at the surface is zero. A radiation condition is used at the seaward boundary to ensure that transient surface gravity waves pass outward through the boundary with no reflection. The seaward condition on density, which does not influence the solution over the shelf, is derived from $w = 0$ and $\partial\tau_{ys}/\partial x = 0$ at $x = -L$, which gives $\partial^2\rho/\partial x^2 = 0$ (Hamilton and Rattray, 1978). Surface and bottom stress are computed from

$$\tau_s = C_D\rho_a|\mathbf{W}|\mathbf{W} \quad \text{and} \quad \tau_b = k\rho|\mathbf{V}|\mathbf{V},$$

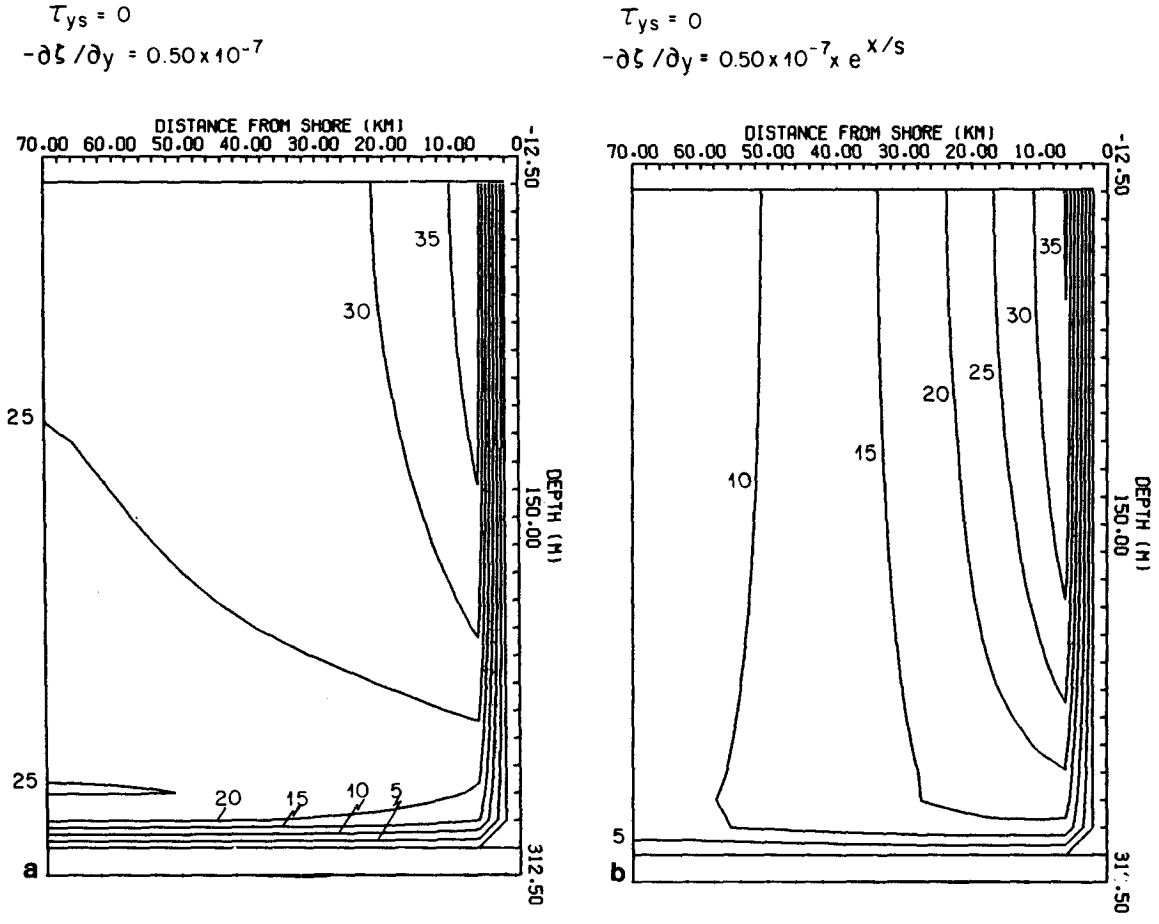

FIG. 1. Contours of longshore velocity (cm s^{-1}) generated by (a) an x and z independent northward longshore pressure gradient force, and (b) a z-independent, but x-dependent, northward longshore pressure gradient force. The flow is northward throughout.

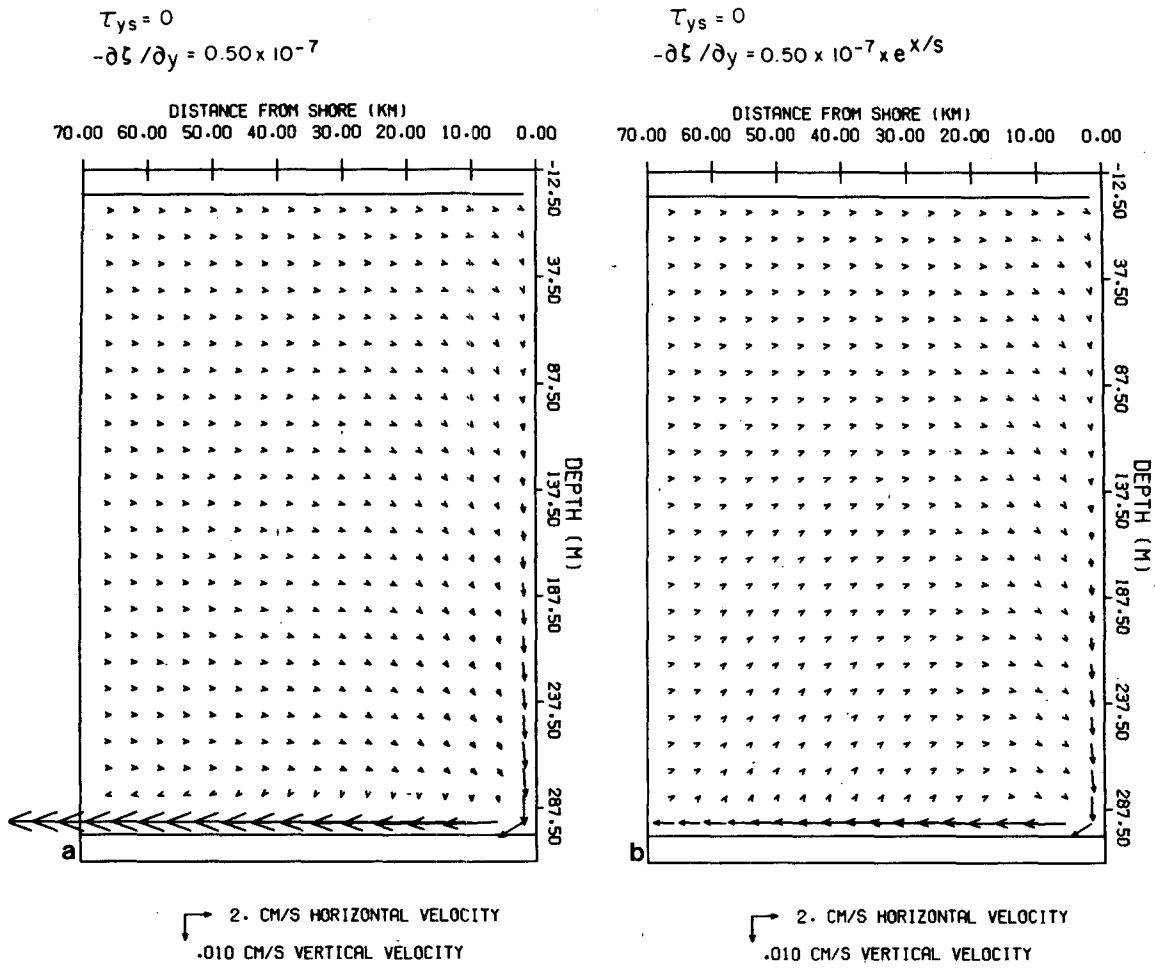

FIG. 2. Cross-shore circulation corresponding to conditions given for Figs. 1a and 1b.

respectively, where $k = 0.0025$, **W** is the wind stress vector, ρ_a the density of air, and **V** the bottom velocity vector. For the summer circulation C_D was set to 0.0013. For the winter and spring circulation C_D was set to 0.0025. Hickey and Hamilton (1980) found that the larger drag coefficient was required to reproduce the observed energy levels in longshore current fluctuations during winter and spring of 1975. The larger coefficient presumably reflects the increased surface roughness scales induced by the large amplitude surface waves that occur during that period.

The vertical and cross-shore structure of the longshore pressure gradient along the Washington–Oregon shelf has not been experimentally determined. Winant (1979) showed that for parameter ranges observed off the west coast of the United States, Csanady's (1978) model would yield cross-shelf trapping scales of the order of the shelf width for wind-induced longshore pressure gradients. On the other hand, Csanady showed that longshore pressure gradients imposed on the coastal region due to deep ocean currents are constant in the cross-shore direction. Unless otherwise stated, we have modulated the $g(\partial\zeta/\partial y)$ term by a factor of $e^{x/s}$, where $s = 40$ km is representative of the shelf width off the Washington coast. Since Hickey and Pola (1982) suggest that the longshore pressure gradient in summer may be due, at least in part, to deep ocean currents, the summer experiments are shown both with and without the coastal-trapping factor.

The structure of the longshore sea level elevation field of Reid and Mantyla (1976) did not change significantly when calculated relative to the 500, 1000 and 2000 db levels. This suggests that the longshore slope of the sea surface might be compensated by the underlying density field above the 500 db level. The relatively good agreement between modeled and observed flow fields demonstrated in Section 5 suggests that over the shallow depths ($\leq$300 m) considered in this study, the assumption of a depth-independent pressure gradient is reasonable and, hence, that compensation takes place below this depth. A linear decay to zero at 200 m (the approximate depth of the shelf break), on the other hand, fails to produce essential

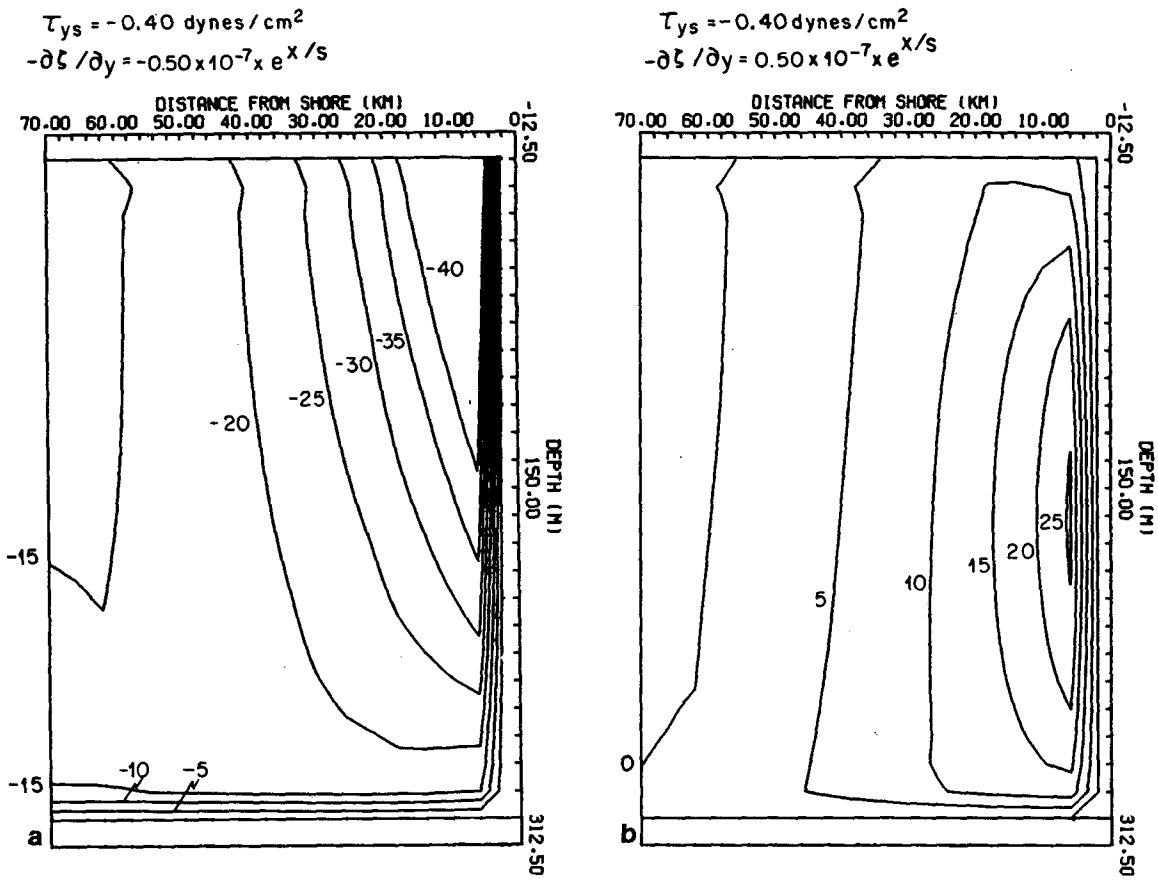

FIG. 3. Contours of longshore velocity (cm s^{-1}) generated by (a) southward wind stress and southward x-dependent (z-independent) longshore pressure gradient force, and (b) southward wind stress and northward x-dependent (z-independent) longshore pressure gradient force. The flow is northward throughout.

features of the observed flow field such as the summer northward shelf-slope undercurrent (not shown).

The equations are solved using a semi-implicit finite difference scheme, forward in time, with a time step of 0.5 h. Horizontal and vertical grid spacings are 4 km and 12.5 m, respectively, and the grid is staggered and centered in space. Horizontal diffusivity is set at 10^6 cm^2 s^{-1}. Vertical eddy diffusivity and viscosity coefficients were formulated as a function of Richardson number according to Munk and Anderson (1948) (see Hamilton and Rattray, 1978).

At the start of each run the velocity field is set to zero and the isopycnals are flat. All cases were run for fortnightly scales to allow initial transients to propagate out of the system. The initial stratification for the experiments which illustrate the basic model response (Section 4) is linear and increases from $\sigma_t = 23$ at the surface to $\sigma_t = 27$ at the bottom.

4. The model response

a. *The elementary response (flat bottom shelf)*

In the absence of a longshore pressure gradient force, the effect of longshore-wind forcing (constant in the cross-shore direction) is to accelerate the water column in the direction of the wind stress until the flow is balanced by bottom stress. In the uniform density case, the steady-state longshore flow will be constant with depth and across the shelf, except in the side-wall and bottom boundaries where frictional effects become important. The steady-state cross-shore circulation is confined to the frictional layers, achieving two-dimensional mass balance in accordance with classical Ekman theory. In the Northern Hemisphere this results in upwelling when the wind is northerly along the eastern boundary of oceans and downwelling when the wind is southerly. When stratification is included, a vertically sheared geostrophic coastal jet develops due to the cross-shore sea surface slope induced by the coastal divergence and the compensatory density field deformation (see Hamilton and Rattray, 1978).

In the absence of wind stress and away from boundary layers, a steady x- and z-independent longshore pressure gradient also initially accelerates longshore flow. As with wind stress forcing, bottom stress increases as the flow accelerates and a corresponding bottom Ekman layer develops. When a steady state

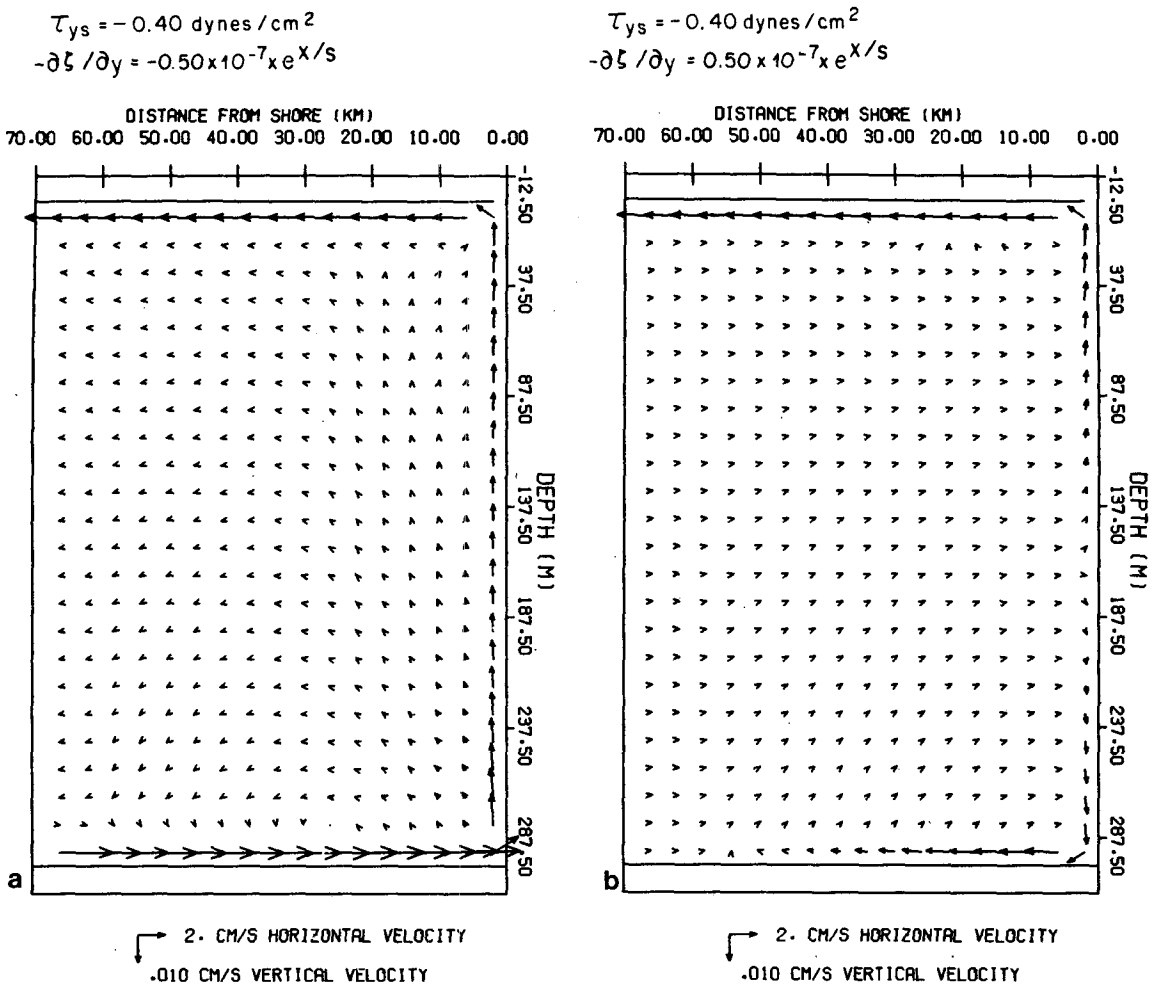

FIG. 4. Cross-shore circulation corresponding to conditions given for Figs. 3a and 3b.

is reached, the longshore flow is in geostrophic balance with the cross-shore sea surface and density field deformations, the interior cross-shore flow is geostrophically balanced by the longshore pressure gradient and two dimensional mass balance is achieved through the bottom Ekman layer. The vertically-integrated longshore momentum balance with two-dimensional mass balance then reduces to

$$0 = -gH\frac{\partial \zeta}{\partial y} - \tau_{yb}. \tag{4.1}$$

A northward pressure gradient force induces northward longshore flow (Fig. 1a). The corresponding onshore flow is depth independent. It impinges on the coastal wall, turns downward and exits through the bottom boundary layer (Fig. 2a). To accommodate the increase of onshore mass flux with depth, vertical velocities near the wall increase in magnitude from the surface layer to the top of the bottom frictional layer in contrast to the relatively depth-independent magnitude of the vertical velocities induced by a longshore wind. When the direction of the pressure gradient force is reversed, as with wind forcing, the flow directions are reversed.

When a longshore pressure gradient force that decays exponentially in the offshore direction is considered, Eq. (4.1) at a distance x from the coast becomes

$$0 = -gHe^{x/s}\frac{\partial \zeta}{\partial y} - \tau_{yb}. \tag{4.2}$$

The basic circulation is the same as for the previous case. The principal differences are that the velocity components are reduced in magnitude, the cross-shore shear of the longshore flow is increased (Fig. 1b) and a vertical velocity is imposed on the velocity field to balance the divergence of the onshore flow. Although difficult to see in Fig. 2b, w is upward in the inviscid interior, decreasing in magnitude between the top of the bottom Ekman layer and the surface, i.e., $\partial w/\partial z$ is negative, balancing the positive $\partial u/\partial x$. At the same time, in the bottom Ekman layer, the cross-shore shear of bottom stress [Eq. (4.2)] results in a convergence of mass and consequent pumping of fluid out of the Ekman layer (Fig. 2b).

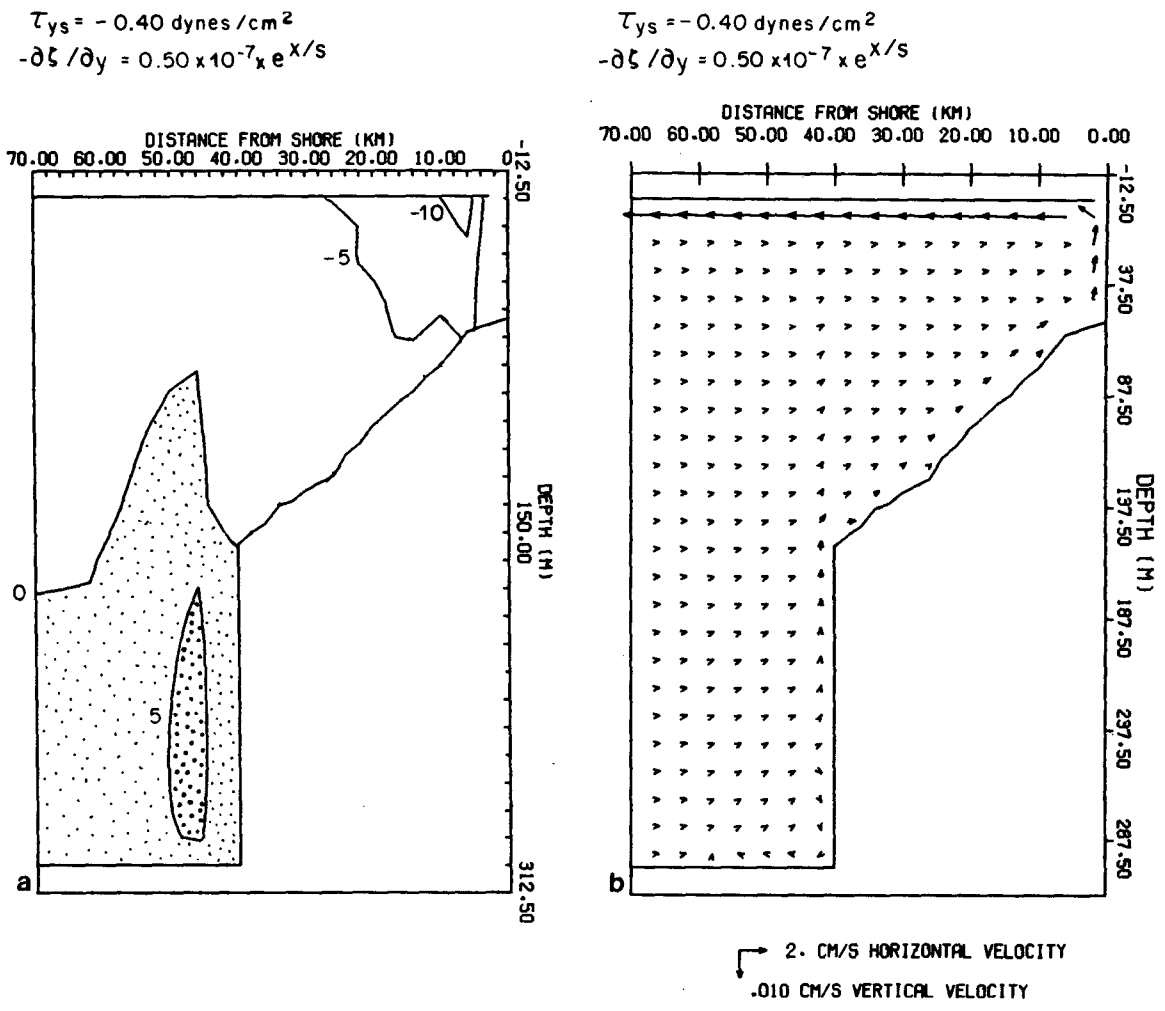

FIG. 5. Contours of longshore velocity (cm s^{-1}) generated by the same conditions as in Fig. 3b, but with bottom topography included. Dots indicate regions of northward flow. (b) Cross-shore circulation corresponding to conditions as in Fig. 5a.

The signature of the cross-shore circulation on the density field is predictable from the circulation pattern. A wind stress favorable for upwelling (or southward pressure gradient force) causes upwarping of the isopycnals near the coastal wall. The displacement of the isopycnals is proportional to the magnitude of the vertical velocity. Therefore, for wind-driven upwelling, the upwarping of the density surfaces is uniform with depth (since the sidewall layer flux is fed mainly through the bottom layer); whereas, for pressure-gradient force-driven upwelling, isopycnal upwarping increases with depth (not shown).

Having established the nature of the response to a longshore wind stress or a pressure gradient force acting individually, we can now easily interpret the response to the simultaneous imposition of these two forces. If the longshore wind stress and the pressure gradient force are both southward, the longshore flow will accelerate southward until the resulting bottom stress is sufficient to balance both forces (Fig. 3a). The cross-shore flow will be offshore near the surface due to both wind stress and pressure gradient, offshore in the interior due to the pressure gradient force, and onshore in a bottom frictional layer to balance the offshore transport above it (Fig. 4a). Note that the bottom layer must generate sufficient transport to balance the offshore flow that occurs over the entire water column; hence its high velocity.

If the longshore pressure-gradient force and wind stress oppose each other, for example, the former is northward and the latter southward, the resulting circulation is more interesting. The cross-shore sea surface slope is a combination of the coastal depression induced by the wind stress and the pile-up due to the longshore pressure gradient. Effectively, the barotropic mode developed in response to the wind is reduced, as shown also by Hurlburt and Thompson (1973). The increase with depth of the pressure-gradient-induced downwelling velocities results in a reversal from upwelling to downwelling at a depth dic-

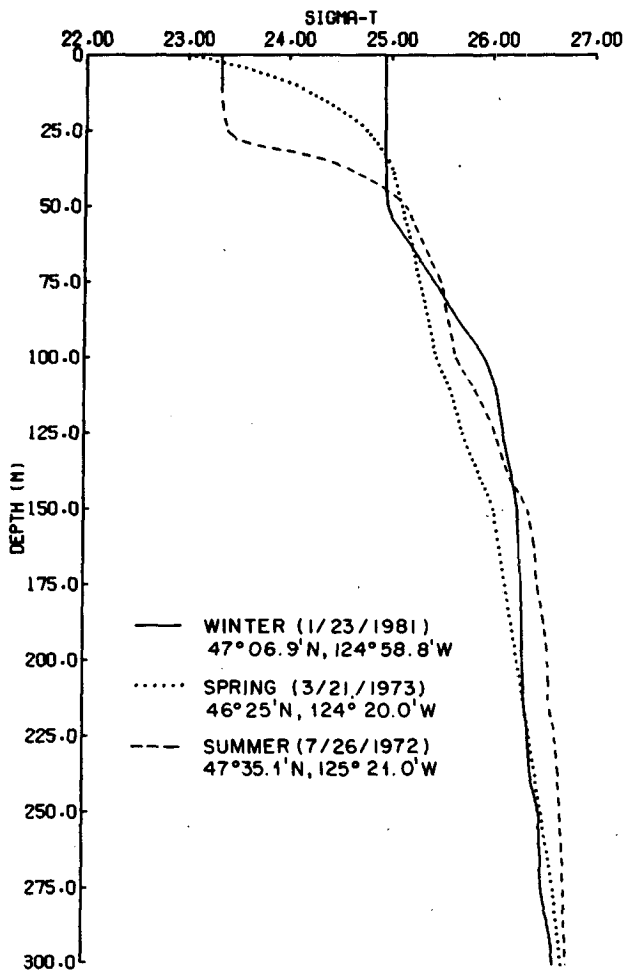

FIG. 6. Initial density profiles used for winter, spring and summer simulations.

tated by the relative magnitudes of the wind stress and the pressure gradient and by the stratification (Fig. 4b). This causes a bifurcation in the density surfaces which, when combined with the inhibition of the barotropic mode, results in a northward geostrophic longshore current at depth, i.e., an undercurrent (Fig. 3b). Without the isopycnal bifurcation, the undercurrent does not develop a core, which is a persistent feature of the west coast summer northward undercurrent (Hickey, 1979).

b. *Topographic effects*

The study of the effect of topography can be subdivided into three cases (all of which are driven by a spatially uniform wind stress): 1) both depth H and longshore pressure gradient force $-g(\partial\zeta/\partial y)$, x-independent; 2) x-dependent H and x-independent $-g(\partial\zeta/\partial y)$, and 3) both H and $-g(\partial\zeta/\partial y)$ x-dependent. Inspection of the steady, vertically integrated longshore momentum equation

$$0 = -gH\frac{\partial\zeta}{\partial y} + \tau_{ys} - \tau_{yb}, \qquad (4.3)$$

reveals that the *direction* of the longshore flow is determined by the requirement that bottom friction balance the wind stress and vertically integrated pressure gradient. In the case where both H and $g(\partial\zeta/\partial y)$ are x-independent, the direction will also be x-independent. However, if H is a function of x, the longshore current will vary in accordance with (4.3); e.g., in shallow water, where wind stress is greater than the vertically integrated pressure gradient force, bottom stress will oppose wind stress and the longshore current will be in the direction of the wind stress. As H increases, the vertically integrated pressure gradient force will eventually become larger than the wind stress and hence bottom stress will oppose the pressure gradient force. Thus bottom stress and longshore current will be zero along an isobath where wind stress and vertically integrated pressure gradient forces balance each other and will change direction as this isobath is crossed (Csanady, 1981). Lastly, if both H and $g(\partial\zeta/\partial y)$ are functions of x, the increase of H with depth is compensated by the decrease of $g(\partial\zeta/\partial y)$ and a result similar to the first case could occur; i.e., the bottom stress as well as the direction of the longshore flow may be relatively constant across the shelf. In Fig. 5a, where results corresponding to the third case are shown, the longshore flow is in the direction of the wind stress across the shelf and an undercurrent develops over the shelf break-slope region due to the mechanisms described in the previous section. In a cross-shore sense, a bifurcation of the flow still occurs (Fig. 5b) although the point of bifurcation occurs below the shelf break.

5. Seasonal variation of the flow

In this section, the winter, spring and summer velocity fields off the Washington–Oregon coast are examined in terms of how they are affected by the barotropic longshore pressure gradient force. The results show that without this force, important features of the circulation over the shelf, shelf-break and slope regions cannot be reproduced.

To allow the most rigorous test of the assumptions in the model formulation, in the spatial structure of the pressure gradient force and in the pressure gradient force data itself, the model simulations are made during periods when current meter data are available for direct comparisons. Winter conditions are simulated for December 1980; spring conditions, for March 1973; and summer conditions for July–August 1972. In each case, we have used the quasi-absolute (de-meaned subsurface pressure data plus long term 0/500 db steric height data) mean monthly pressure gradient data from Hickey and Pola (1982), non-seasonal pressure gradient anomalies from Enfield and Allen (1980) [not available in 1980] and

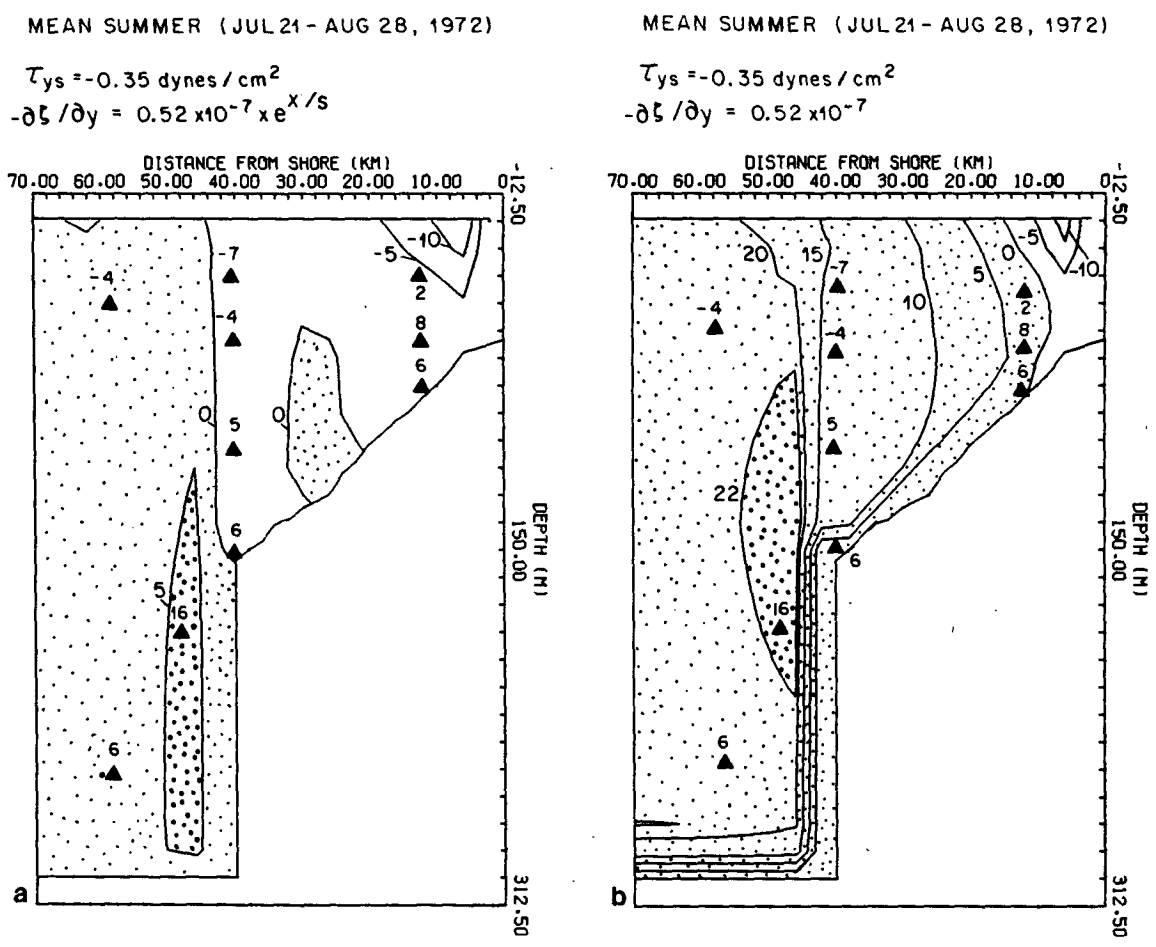

FIG. 7. (a) Contours of longshore velocity (cm s^{-1}) generated by observed mean wind stress and observed mean longshore pressure gradient force for 21 July to 28 August 1972. (b) As in Fig. 7a, except that the longshore pressure gradient force is constant in the cross-shore direction. Dots indicate regions of northward flow. Numbers next to triangles are observed mean longshore velocities (from Hickey, 1979).

hourly (spring) or mean (summer and winter) wind stress data obtained from hourly wind observations at local coastal wind stations during the period being investigated.

Initial stratification profiles during winter and summer were obtained from CTD stations in ~400 m of water taken during the actual period under investigation (Fig. 6). Spring comparisons differ from those of winter and summer in that comparisons are made only over the shelf and in that comparisons are made on three individual days rather than for the mean. To include the effect of the Columbia River effluent, which was present at the time of the observations, the upper 80 m of the initial density profile was taken from data near the mid-shelf current meter mooring. The remainder of the profile consisted of two segments: 80–200 m data were taken from an outer shelf profile obtained the same day as the mid-shelf profile; 200–300 m data were taken from the historical mean for spring at this location (McGary, 1971).

1) SUMMER

The principal oceanographic features for the Pacific Northwest shelf and slope regions during summer are well-documented: southward wind stress, northward pressure gradient force (Hickey and Pola, 1982), near-surface southward flow and strong baroclinic shear over the mid- and outer shelf and slope resulting in northward near-bottom flow (Huyer *et al.*, 1978; Hickey, 1979). The most remarkable feature of the circulation is a narrow (~10 km) jet-like northward undercurrent that occurs just below the shelf break (Hickey, 1979). This undercurrent, which is called the California Undercurrent, occurs along the West Coast from California to Vancouver Island; alongshore continuity has not been fully established. The undercurrent increases in strength from early to late summer. Although several wind-driven models have predicted undercurrents (e.g., McCreary, 1981; Yoon and Philander, 1982), the analysis of Hickey

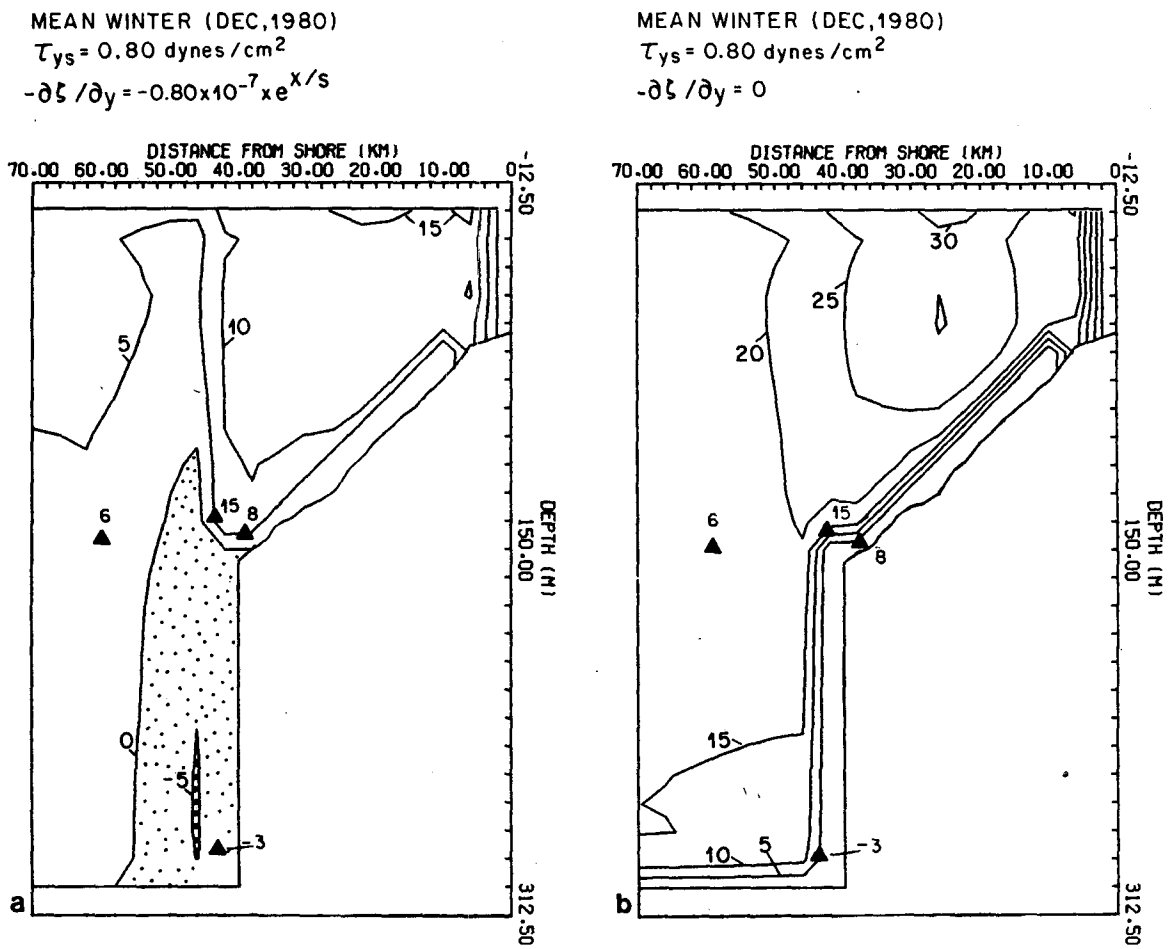

FIG. 8. (a) Contours of longshore velocity (cm s^{-1}) generated by observed mean wind stress and observed mean longshore pressure gradient force for December 1980. Dots indicate regions of southward flow. Numbers next to triangles are observed mean longshore velocities. (b) Contours generated by the wind stress used for results of Fig. 8a. The flow is northward throughout.

and Pola, which compares the results of a wind-driven model (Csanady, 1978) and a deep ocean current model to observed sea surface slope, demonstrates that large-scale (widths of several hundred kilometers) deep ocean currents also contribute substantially to the seasonal alongshore pressure gradient. In particular, sea level in the Pacific Northwest is anomalously low in comparison with that predicted by the wind-driven model alone, from July to September so that the actual pressure gradient force and, hence, the strength of the undercurrent, is larger than that predicted by wind-driven coastal models. Thus, a model in which the pressure gradient is treated as an external force should more accurately predict the summer flow field in the Pacific Northwest.

Figs. 7a and b display the longshore velocity field for the model (contoured) and the observations for the period 21 July–28 August. In view of Hickey and Pola's conclusions about the importance of deep ocean currents during summer, the model was run both with (Fig. 7a) and without (Fig. 7b) the coastal trapping factor ($e^{x/s}$) included in the pressure gradient. The cross-shore velocity field for Fig. 7a resembles Fig. 5b. The principal features of the longshore velocity field are best reproduced by the model without the coastal trapping feature. The southward near-surface flow that is strongest over the outer shelf and slope is not predicted by either model run. This flow may be the shoreward edge of the deep ocean California Current. The results presented in Section 4 illustrate that the northward pressure gradient force is essential to the formation of the subsurface maximum in northward flow.

2) WINTER

Given that the directions of the wind stress and pressure gradient force during winter are opposite to those in summer and given the fact that stratification is only slightly weaker than that in summer (Fig. 6),

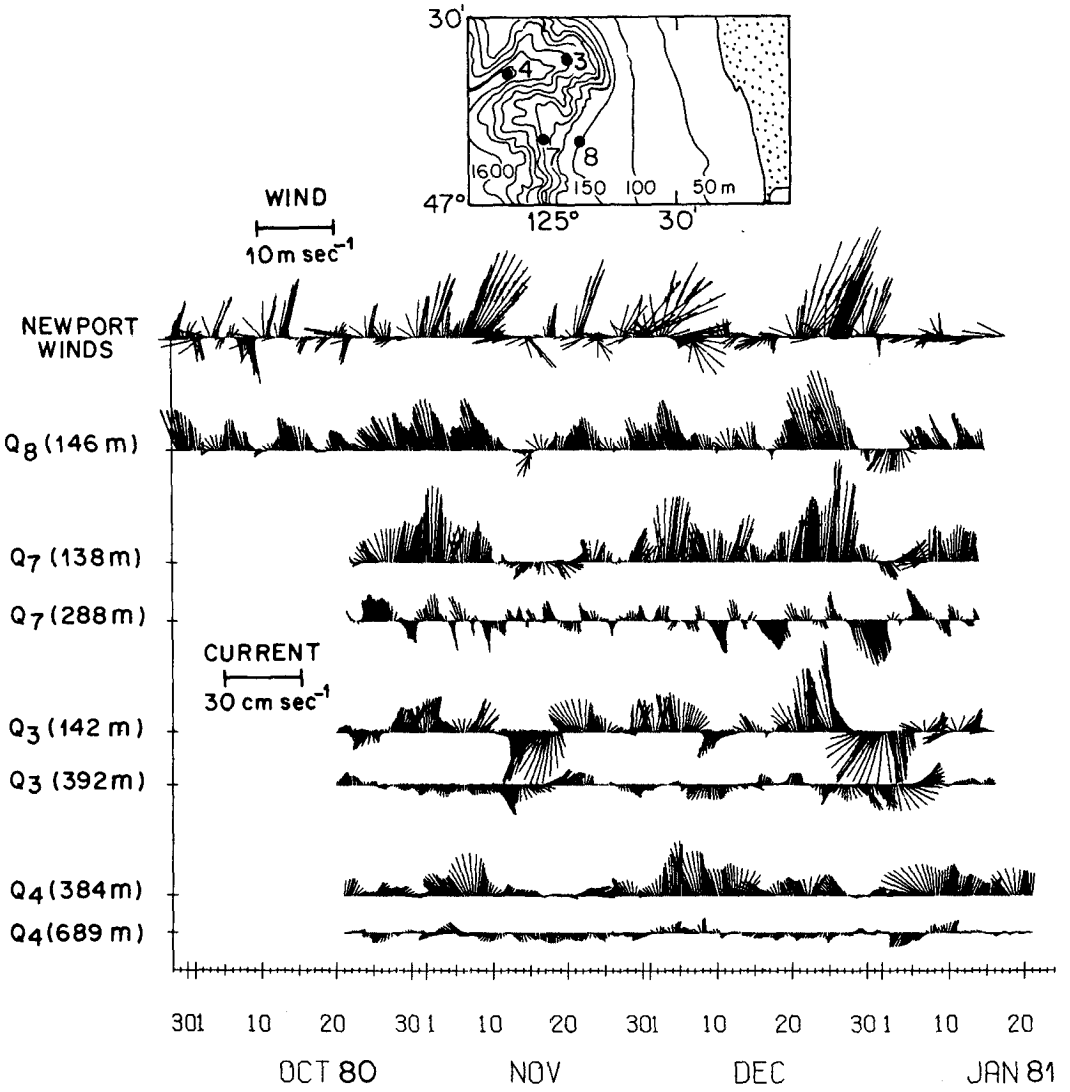

FIG. 9. Observations during fall-winter 1980–81 of winds at Newport, Oregon (45°N) and currents off the Washington coast. Location of the current meter moorings are shown on the bathymetric chart. Data have been filtered to remove tidal and inertial fluctuations.

it is not surprising that the model predicts a southward undercurrent during the winter season (Fig. 8a). Since there have been few slope experiments during the winter, this undercurrent has never been discussed in the literature, although Hickey (1979) states that "there is some evidence for a mean southward offset to the flow over the shelf during winter and spring that is not directly related to wind stress". Indeed, Fig. 12 in Hickey (1979) which illustrates currents over the slope during February and March, 1975 does show a minimum in mean poleward flow at 415 m, relative to that at 65 and 815 m. Additional support for the existence of subsurface southward flow during winter, at least at the shelf edge, can be seen in Smith *et al.* (1976), who show winter records during 1971, 1972, 1973 and 1974. Data taken during October 1980–January 1981 show the undercurrent quite clearly (Fig. 9). Mean longshore velocities during December correspond surprisingly well to those predicted by the model driven by both mean pressure gradient and mean wind stress (Fig. 8a). No southward flow is predicted when only wind stress is used to force the model (Fig. 8b).

3) SPRING

In late winter and early spring an atmospheric high pressure system is set up off the Pacific northwest which causes the winds to change directions from primarily southerly to northerly in a matter of 1–3 days (Sobey, 1977). The reversal in the currents is dramatic, for not only do they become southward

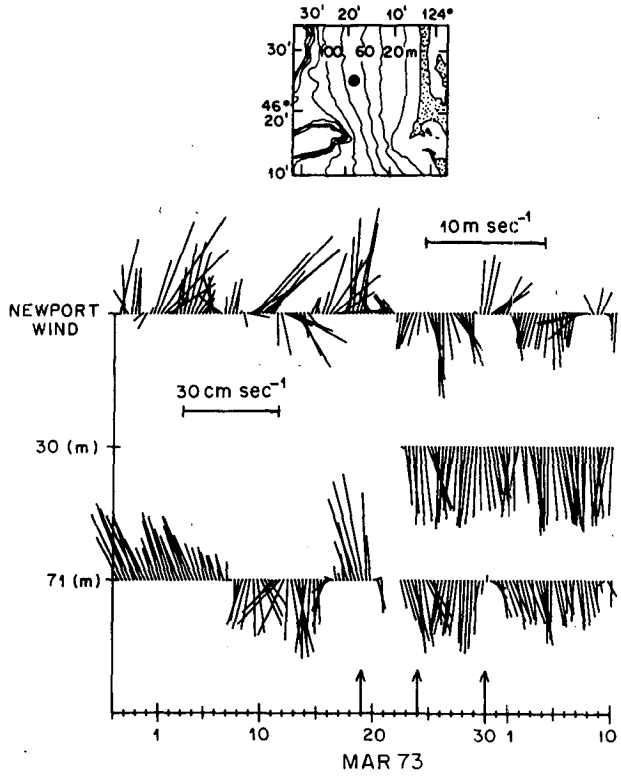

FIG. 10. Observations during March and April 1973 of winds at Newport, Oregon (45°N) and currents off Washington in a bottom depth of 80 m. Location of the current meter mooring is shown on the bathymetric chart. Data have been filtered to remove tidal and inertial fluctuations. Arrows on the time axis indicate dates of model-observation comparisons.

(together with the winds) but they remain southward even when southerly wind events take place. The southward flow that occurs during this period in the Pacific Northwest exceeds that which occurs during summer when local longshore wind stress is strongest (Hickey, 1979). The *onset* of southward flow, which occurs simultaneously over longshore scales of several hundred kilometers, has become known as the "spring transition" [Smith *et al.* (1976) for 1973, and Huyer *et al.* (1979) for 1973 through 1976]. Our model studies will demonstrate that the anomalously strong southward flow that follows the transition can be adequately explained by consideration of the southward longshore pressure gradient force during this period. The existence of the southward pressure gradient force during late winter and early spring also explains the periods of southward flow that occur with increasing frequency prior to the actual transition (see Hickey, 1981).

Velocity data surrounding the transition of 1973 are shown in Fig. 10. The currents over the shelf are primarily northward until 20 March (see also Smith *et al.*, 1976) when they become southward with speeds on the order of 25 cm s^{-1}. The pressure gradient force during March and April is southward as in winter. Thus, when the winds reverse, both surface stress and pressure gradient force are in the same direction. Results of numerical experiments run with the measured hourly winds with and without the measured mean southward longshore pressure gradient force are shown in Figs. 11a and b (19 March, before the transition), Figs. 12a and b (24 March, after the transition) and Figs. 13a and b (during a local northward wind event after the transition). When the model is forced with only wind stress, the flow prior to the transition and just after the transition is more northward than the observations (Figs. 11a and 12a). Including the longshore pressure gradient force in the model produces both northward (before transition, Fig. 11b) and southward (just after transition, Fig. 12b) currents much closer in magnitude to the observations. During the southerly wind event that took place from 28 to 30 March, the observed mid-shelf currents remained strongly southward. Figs. 13a and b show that this result is only predicted when the longshore pressure gradient force is included in the model.

Additional support for the importance of the longshore pressure gradient during this time period can be obtained from considerations of volume changes over the shelf. Huyer *et al.* (1978) estimated a change of 1.27×10^7 cm^3 per centimeter of coastline in the volume of water over the shelf during the 1975 transition. Using the mean wind stress for the eight days surrounding the transition (beginning March 24) of 0.67 dynes cm^{-2} (southward), they calculated a change in volume of 6.95×10^6 cm^3 per centimeter of coastline (based on denser water replacing the lighter water advected offshore due to Ekman dynamics), i.e., they accounted for 55% of the change. The average seasonal mean longshore pressure-gradient force (over a shelf that increases in depth from 55 to 155 m in 40 km, as presently modeled) can be calculated simply from the mean value theorem:

$$\frac{1}{s}\int_0^s -gH(x)e^{x/s}\frac{\partial \zeta}{\partial y}\,dx.$$

The effective southward stress is increased from 0.67 to 1.17 dyn cm^{-2}, thus accounting for a change in volume of 1.21×10^7 cm^3 per centimeter of coastline; i.e., 95% of the change in volume.

FIG. 11. (a) Contours of longshore velocity (cm s^{-1}) generated by observed hourly winds from 10 to 19 March 1973. Numbers next to triangles are observed mean longshore velocities for 19 March. (b) As in (a), but including observed mean longshore pressure gradient force. Dots indicate regions of southward flow.

FIG. 12. (a) Contours of longshore velocity (cm s^{-1}) generated by observed hourly winds from 10 to 24 March 1973. Dots indicate regions of southward flow. Numbers next to triangles are observed mean longshore velocities for 24 March. (b) As in (a), but including observed mean longshore pressure gradient force.

MARCH 19 , 1973

τ_{ys} = NEWPORT HOURLY

$-\partial\zeta/\partial y = 0$

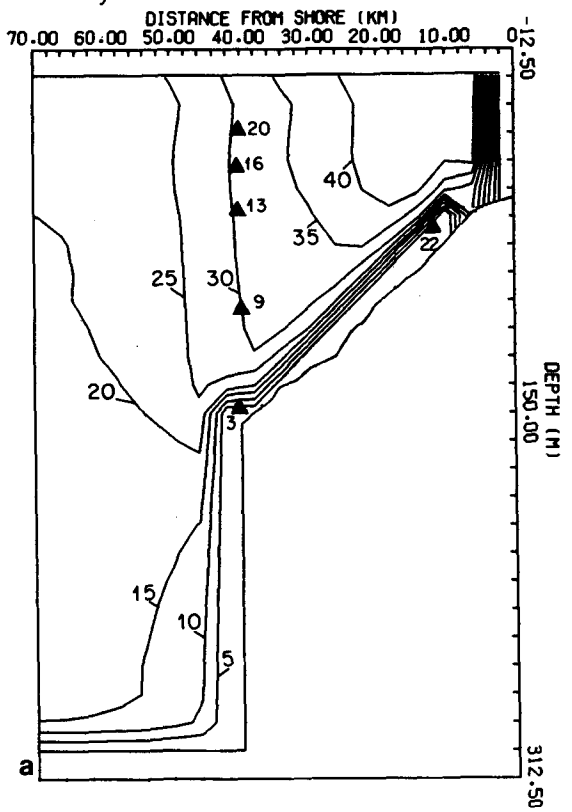

MARCH 19 , 1973

τ_{ys} = NEWPORT HOURLY

$-\partial\zeta/\partial y = -0.81 \times 10^{-7} \times e^{x/s}$

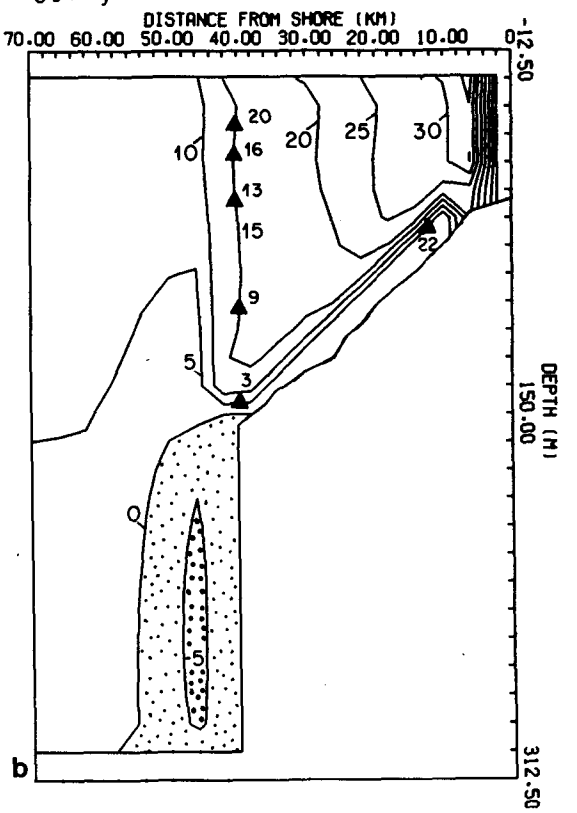

MARCH 24 , 1973

τ_{ys} = NEWPORT HOURLY

$-\partial\zeta/\partial y = 0$

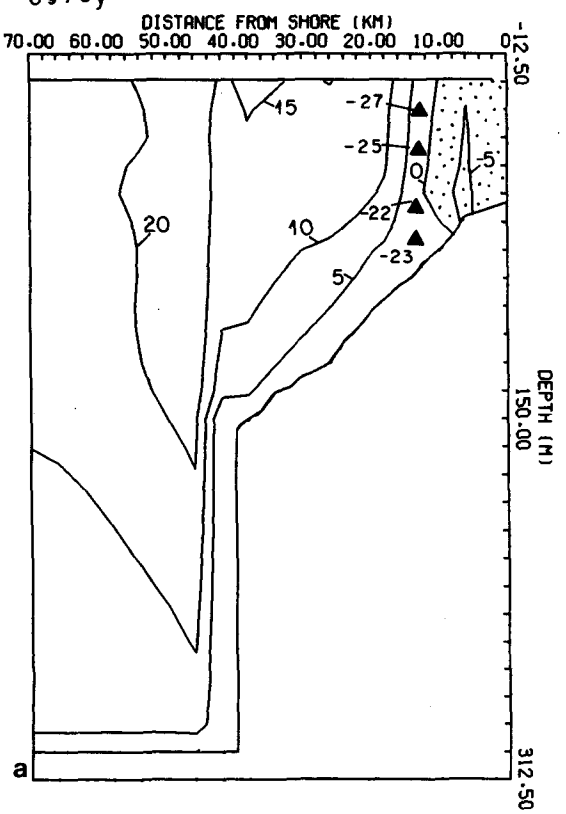

MARCH 24 , 1973

τ_{ys} = NEWPORT HOURLY

$-\partial\zeta/\partial y = -0.81 \times 10^{-7} \times e^{x/s}$

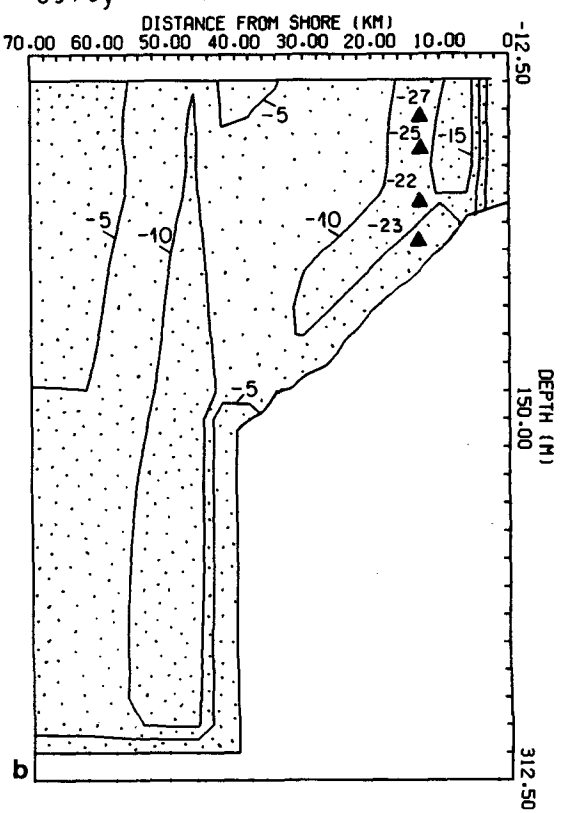

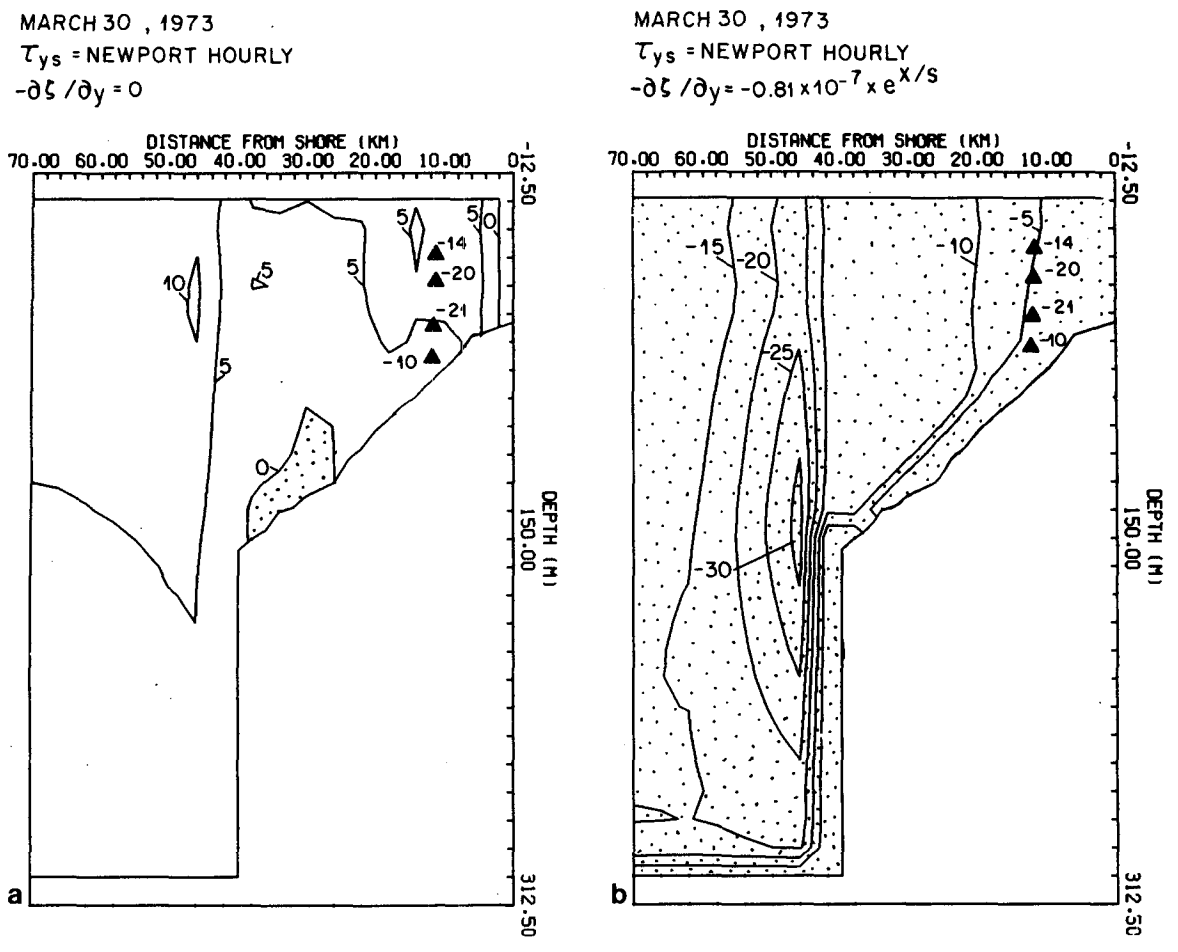

FIG. 13. (a) Contours of longshore velocity (cm s^{-1}) generated by observed hourly winds from 10 to 30 March 1973. Dots indicate regions of southward flow. Numbers next to triangles are observed mean longshore velocities for 30 March. (b) As in (a), but including observed mean longshore pressure gradient force.

6. Discussion

The results of the preceding sections allow us to quantify the principal terms in the momentum equations as a function of season and of distance offshore. Values of surface and bottom stress and of the vertically integrated longshore pressure gradient force for mid-shelf bottom depths and for depths below the shelf break have been calculated from the model results for each season and are illustrated in Fig. 14, along with the longshore current directions derived from the model results. The balance in the inner shelf region was inferred from the discussion by Csanady (1981). Whereas the winter and summer cases represent steady state solutions, the spring data are time-dependent. The conditions on 24 March are taken to represent a typical early spring situation. The figure illustrates that the importance of the longshore pressure gradient force increases with bottom depth. In winter and summer, when surface stress and vertically integrated pressure gradient force oppose each other, the direction of bottom stress in the very nearshore region opposes that in the offshore region. Bottom stress is significant on the inner shelf during summer and on the inner and mid-shelf during winter. It is not significant in mid-shelf regions during summer, as shown also by Allen and Kundu (1978) and Allen and Smith (1981). During spring when it must balance both surface stress and pressure gradient force, bottom stress is significant at all depths.

Last, we address the question of the value of $\int_0^H fudz$. It is often assumed (see, e.g., Enfield and Allen, 1980) that transport in the surface Ekman layer is balanced by onshore transport in the inviscid interior. Our results indicate that whereas this assumption is reasonably valid for mean summer conditions on the mid- and outer shelf, it is not appropriate during spring and winter when a very strong bottom Ekman layer develops in conjunction with the strong southward or northward flow, respectively. In summer 1972, onshore transport in the bottom layer on the shelf was several orders of magnitude less than offshore transport in the surface layer. In spring 1973, however, the bottom onshore transport (0.4×10^4 cm^2 s^{-1}) balanced the surface offshore transport (-0.4×10^4 cm^2 s^{-1}) in the mid-shelf region. The results

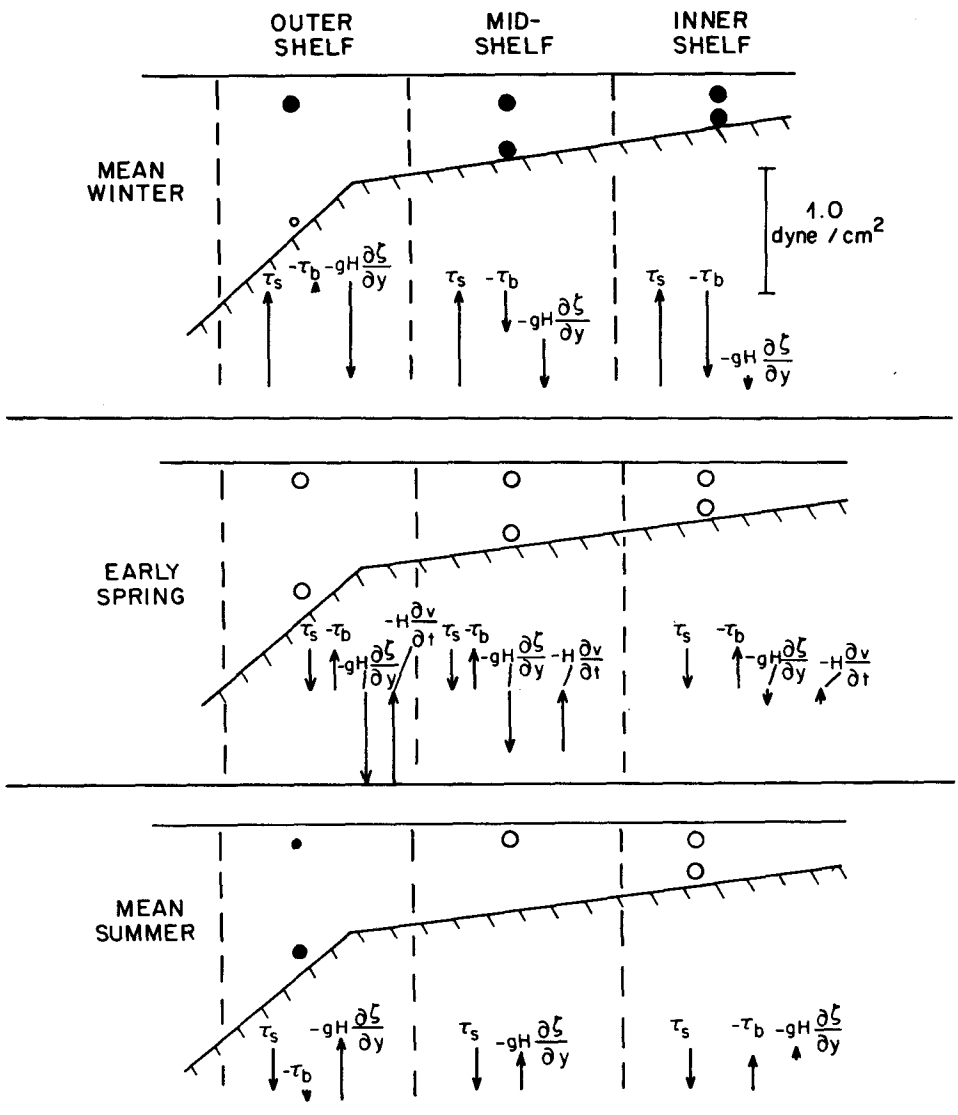

FIG. 14. Seasonal variation of momentum balance in the Pacific Northwest coastal zone including wind stress, longshore pressure gradient force and bottom stress for mean winter and mean summer conditions and for 24 March 1973, the day following the spring transition. Solid dots indicate northward flow (into the page). Mean summer results are those derived with the coastal trapping factor included (Fig. 7a).

from the mean winter simulation were intermediate between the spring and summer results; namely, the bottom offshore transport (-0.3×10^4 cm^2 s^{-1}) was about one third the surface onshore transport (0.8×10^4 cm^2 s^{-1}). Additional support for the importance of the bottom Ekman layer during winter months on the Washington shelf can be found in Smith and Long (1976) where the role of the bottom layer in transporting sediment offshore as well as its importance in achieving mass balance on the shelf was clearly established.

Acknowledgments. We wish to thank Dr. Peter Hamilton for the use of his computer coding. This work was supported by the Department of Energy under Contract DE-AT06-76-EV-71025-14 and by the National Science Foundation under Grant OCE 79-19252.

APPENDIX

List of Symbols

x, y, z — a right-handed coordinate system with x positive eastward (onshore), y northward and z upward; the undisturbed sea surface is given by $z = 0$, and the bottom by $z = -h(x)$; the coast is at $x = 0$ and the seaward boundary is at $x = -L$. We refer to x and y as the cross-shore and longshore directions, respectively.

u, v, w	the velocity components in the x, y, z directions, respectively
$\bar{u}, \bar{v}$	the depth-averaged velocities given by $\bar{u} = H^{-1} \int_{-h}^{\zeta} u dz$ (and similarly for $\bar{v}$)
t	time
ζ	free surface elevation above the undisturbed surface
ρ, ρ_0	density, mean density
g	acceleration due to gravity
f	Coriolis parameter
H	total depth $[=h + \zeta]$
A_v	vertical eddy viscosity coefficient
K_v, K_h	vertical and horizontal eddy diffusion coefficients
$\tau_{xs}, (\tau_{ys})$ $\tau_{xb}, (\tau_{yb})$	surface and bottom stresses in the x, (y) direction, respectively.

REFERENCES

Allen, J. S., and P. K. Kundu, 1978: On momentum, vorticity and mass balance on the Oregon Shelf. *J. Phys. Oceanogr.*, **8,** 13–27.

——, and R. L. Smith, 1981: On the dynamics of wind-driven shelf currents. *Phil. Trans. Roy. Soc. London,* **A302,** 617–634.

Brink, K. H., 1982: The effect of bottom friction on low-frequency coastal trapped waves. *J. Phys. Oceanogr.*, **12,** 127–133.

Bryden, H. L., 1978: Mean upwelling velocities on the Oregon Continental Shelf during summer 1973. *Estuar. Coastal Mar. Sci.*, **7,** 311–327.

Csanady, G. T., 1978: The arrested topographic wave. *J. Phys. Oceanogr.*, **8,** 47–62.

——, 1981: Circulation in the coastal ocean. *Advances in Geophysics,* Vol. 23, Academic Press, 101–183.

Enfield, D. B., and J. S. Allen, 1980: On the structure and dynamics of monthly mean sea level anomalies along the Pacific Coast of North and South America. *J. Phys. Oceanogr.*, **10,** 557–578.

Garvine, R. W., 1971: A simple model of coastal upwelling dynamics. *J. Phys. Oceanogr.*, **1,** 169–179.

Hamilton, P., and M. Rattray, Jr., 1978: A numerical model of the depth dependent, wind-driven upwelling circulation on a continental shelf. *J. Phys. Oceanogr.*, **8,** 437–457.

Hickey, B. M., 1979: The California Current System—hypotheses and facts. *Prog. Oceanogr.*, **8,** 191–279.

——, 1981: Alongshore coherence on the Pacific Northwest continental shelf (January–April, 1975). *J. Phys. Oceanogr.*, **11,** 822–835.

——, and P. Hamilton, 1980: A spin-up model as a diagnostic tool for interpretation of current and density measurements on the continental shelf of the Pacific Northwest. *J. Phys. Oceanogr.*, **10,** 12–24.

——, and N. Pola, 1982: The alongshore pressure gradient on the west coast of the United States. *J. Geophys. Res.* (in press).

Hurlburt, H. E., and J. D. Thompson, 1973: Coastal upwelling on a β-plane. *J. Phys. Oceanogr.*, **3,** 16–32.

Huyer, A., R. L. Smith and E. C. J. Sobey, 1978: Seasonal differences in low frequency current fluctuations over the Oregon continental shelf. *J. Geophys. Res.*, **83,** 5076–5089.

——, E. C. J. Sobey and R. L. Smith, 1979: The spring transition in currents over the Oregon continental shelf. *J. Geophys. Res.*, **84,** 6995–7011.

McCreary, J. P., Jr., 1981: A linear stratified ocean model of the coastal undercurrent (a model of the coastal undercurrent). *Phil. Trans. Roy. Soc. London,* **A302,** 385–415.

McGary, N. B., 1971: *An Atlas of the Columbia River Effluent and its Distribution at Sea.* University of Washington, Dept. Oceanogr., Special Report, No. 47, 57 pp.

Montgomery, R. B., 1941: Transport of the Florida Current off Havana. *J. Mar. Res.*, **4,** 198–219.

Munk, W. H., and E. R. Anderson, 1948: Notes on a theory of the thermocline. *J. Mar. Res.*, **7,** 276–295.

Philander, S. G. H., and J. H. Yoon, 1982: Eastern boundary currents and coastal upwelling. *J. Phys. Oceanogr.*, **12,** 862–879.

Reid, J. L., Jr., and A. W. Mantyla, 1976: The effect of the geostrophic flow upon coastal sea elevations in the northern North Pacific Ocean. *J. Geophys. Res.*, **81,** 3100–3110.

Scott, J. T., and G. T. Csanady, 1976: Nearshore currents off Long Island. *J. Geophys. Res.*, **81,** 5401–5409.

Smith, J. D., and C. E. Long, 1976: Near bottom flow and sediment transport. *Mém. Soc. R. Sci. Liege,* 6th Ser., **10,** 369–396.

——, B. Hickey and J. Beck, 1976: Observations from moored current meters on the Washington continental shelf from February 1971–February 1974. University of Washington, Dept. Oceanogr., Special Report. No. 65, 383 pp.

Sobey, E. C. J., 1977: The response of Oregon shelf waters to wind fluctuations: Differences and the transition between winter and summer. Ph.D. dissertation, Oregon State University, 153 pp.

Stommel, H., and A. Leetmaa, 1972: The circulation on the continental shelf. *Proc. Nat. Acad. Sci. U.S.*, **69,** 3380–3384.

Suginohara, N., 1982: Coastal upwelling: Onshore-offshore circulation, equatorward coastal jet and poleward undercurrent over a continental shelf slope. *J. Phys. Oceanogr.*, **12,** 272–284.

Welander, P., 1957: Wind action on a shallow sea: Some generalizations of Ekman's theory. *Tellus,* **9,** 45–52.

Winant, C. D., 1979: Comments on "The arrested topographic wave." *J. Phys. Oceanogr.*, **9,** 1042–1043.

Yoon, J. H., and S. G. H. Philander, 1982: The generation of coastal undercurrents. *J. Oceanogr. Soc. Japan,* **38,** 215–224.

Yoshida, K., 1967: Circulation in the eastern tropical oceans with special references to upwelling and undercurrents. *Japan J. Geophys.*, **4,** 1–75.